Available at: http://publications.ictp.it IC/2008/050

United Nations Educational, Scientific and Cultural Organization
and
International Atomic Energy Agency
THE ABDUS SALAM INTERNATIONAL CENTRE FOR THEORETICAL PHYSICS

NEUTRINO ENERGY LOSS RATES DUE TO KEY IRON ISOTOPES FOR CORE-COLLAPSE PHYSICS

Jameel-Un Nabi[1]
Faculty of Engineering Sciences, GIK Institute of Engineering Sciences and Technology, Topi 23640, Swabi, NWFP, Pakistan
and
The Abdus Salam International Centre for Theoretical Physics, Trieste, Italy.

Abstract

Accurate estimates of neutrino energy loss rates are needed for the study of the late stages of the stellar evolution, in particular for the cooling of neutron stars and white dwarfs. The energy spectra of neutrinos and antineutrinos arriving at the Earth can also provide useful information on the primary neutrino fluxes as well as neutrino mixing scenario. Proton-neutron quasi-particle random phase approximation (pn-QRPA) theory has recently being used for a microscopic calculation of stellar weak interaction rates of fp-shell nuclide, particularly iron isotopes, with success. Here I present the calculation of neutrino and antineutrino energy loss rates due to key iron isotopes in stellar matter using the pn-QRPA theory. The rates are calculated on a fine grid of temperature-density scale suitable for core-collapse simulators. The calculated rates are compared against earlier calculations. The neutrino cooling rates due to even-even isotopes of iron, ^{54,56}Fe, are in good agreement with the rates calculated using the large-scale shell model. The pn-QRPA calculated neutrino energy loss rates due to ^{55}Fe are enhanced roughly around an order of magnitude compared to the large-scale shell model calculation during the oxygen and silicon shell burning stages of massive stars and favor a lower entropy for the cores of massive stars.

MIRAMARE – TRIESTE
July 2008

[1]Junior Associate of ICTP. jnabi00@gmail.com

1 Introduction

Despite immense technological advancements since the time when Colgate & White [1] and Arnett [2] presented their classical work on energy transport by neutrinos and antineutrinos in non-rotating massive stars, the explosion mechanism of core-collapse supernovae continues to pose challenges for the collapse simulators throughout the globe. It is clear that the prompt shock that follows the bounce of the core stagnates and is not possible to cause a supernova explosion on its own. It loses energy in disintegrating iron nuclei and through neutrino emissions (mainly non-thermal) which are till then transparent to the stellar matter. A few milliseconds after the bounce, the proto-neutron star accretes mass at a few tenths of solar mass per second. This accretion, if continued even for one second, can change the ultimate fate of the collapsing core resulting into a black hole. Neutrinos are the main characters in this play and radiate around 10% of the rest mass converting the star to a neutron star. Initially the nascent neutron star is a hot thermal bath of dense nuclear matter, e^-e^+ pairs, photons and neutrinos. Neutrinos, having the weak interaction, are most effective in cooling and diffuse outward within a few seconds, and eventually escape with about 99% of the released gravitational energy. Despite the small neutrino-nucleus cross sections, the neutrinos flux generated by the cooling of a neutron star can produce a number of nuclear transmutations as it passes the onion-like structured envelope surrounding the neutron star. In the late-time neutrino heating mechanism the stalled shock can be revived (about 1 s after the bounce) and may be driven as a delayed explosion [3]. However to date there have been no successfully simulated spherically symmetric explosions. Even the 2D simulations (addition of convection) performed with a Boltzmann solver for the neutrino transport fails to convert the collapse into an explosion [4]. 2D calculations carried out in the mid -1990's resulted in successful supernovae and revealed some role of turbulence in the collapsing gas (e.g. [5]). Additional energy sources were also sought that might transport energy to the mantle and lead to an explosion. Two such popular sources of additional energy that were widely discussed in literature were magnetic fields (e.g. [6]) and rotations (e.g. [7]).

Yet another popular and much debated energizing mechanism for shock revival is that of "preheating" proposed by Haxton [8]. Haxton suggested that a significant fraction of the energy carried by the neutrinos could be utilized in preheating iron nuclei outside the shock front rather than getting lost. This would lead to a reduction in the energy required from the shock wave to dissociate the infalling Fe, assisting the shock wave to retain more of its strength as it propagates through the iron core and thus increasing the chances of transforming the collapse into an explosion. Bruenn and Haxton [9] later discouraged the preheating mechanism. They worked on two different models, simulating weak and strong shock cases, and found out that in neither case is the energy transferred to the matter by neutrino-nucleus absorption significant in terms of preheating the infalling iron-like material. More recently, Langanke and collaborators [10] had some observations on the models of Bruenn and Haxton [9] and reported much larger preshock

heating rates than those calculated by Bruenn and Haxton. They concluded that these rates act for too short a time to lead to consequences for shock propagation. Despite all this, the preheating mechanism in fact has been adopted by most coders, who are continually putting in more microphysics to make the simulations more realistic and there continues to be interest in this problem [11].

The structure of the progenitor star has a vital role to play in the mechanism of the explosion. A lot many physical inputs are required at the beginning of each stage of the entire simulation process including but not limited to collapse of the core, formation, stalling and revival of the shock wave and shock propagation. It is highly desirable to calculate the presupernova stellar structure with the most reliable physical data and inputs.

Neutrinos from core-collapse supernovae are unique messengers of the microphysics of supernovae and are crucial to the life and afterlife of supernovae. They provide information regarding the neutronization due to electron capture, the infall phase, the formation and propagation of the shock wave and the cooling phase. Cooling rate is one of the crucial parameters that strongly affect the stellar evolution. During the late stages of stellar evolution a star mainly looses energy through neutrinos. White dwarfs and supernovae (which are the endpoints for stars of varying masses) have both cooling rates largely dominated by neutrino production. A cooling proto-neutron star emits about 3×10^{53} erg in neutrinos, with the energy roughly equipartitioned among all species. Further the neutrinos and antineutrinos produced as a result of nuclear reactions are transparent to the stellar matter at presupernova densities and therefore assist in cooling the core to a lower entropy state. This scenario does not necessarily hold at extremely high densities and temperatures (this would be the case for stellar collapse where dynamical time scales become shorter than the neutrino transport time scales) where neutrinos can become trapped in the so-called neutrinospheres mainly due to elastic scattering with nuclei. Prior to stellar collapse one requires an accurate determination of neutrino loss rates in order to perform a careful study of the final branches of star evolutionary tracks. A change in the cooling rates particularly at the very last stages of massive star evolution could affect the evolutionary time scale and the iron core configuration at the onset of the explosion [12]. The electron capture rates and the accompanying neutrino energy loss rates are also required in determining the equation of state. The neutrino energy loss rates are important input parameters in multi-dimensional simulations of the contracting proto-neutron star. Reliable and microscopic calculations of neutrino loss rates and capture rates can contribute effectively in the final outcome of these simulations on world's fastest supercomputers.

The first-ever extensive calculation of stellar weak rates including the capture rates, neutrino energy loss rates and decay rates for a wide density and temperature domain was performed by Fuller, Fowler, and Newman (FFN) [13]. The calculation was done for 226 nuclei in the mass range $21 \leq A \leq 60$. The authors stressed on the importance of the Gamow-Teller (GT) giant resonance strength in the capture of the electron and estimated the GT centroids using zeroth-

order ($0\hbar\omega$) shell model. Later, Aufderheide et al. [14] extended the FFN work for heavier nuclei with A $>$ 60 and took into consideration the quenching of the GT strength neglected by FFN. Authors in Ref. [14] also stressed on the importance of beta decay rates in the iron core prior to the collapse. They tabulated the 90 top electron capture nuclei averaged throughout the stellar trajectory for $0.40 \leq Ye \leq 0.5$ (see Table. 25 therein). The measured data from various (p,n) and (n,p) experiments later revealed the misplacement of the GT centroid adopted in the parameterizations of FFN. Since then theoretical efforts were concentrated on the microscopic calculations of weak-interaction mediated rates of iron-regime nuclide. Large-scale shell model (LSSM)(e.g. [15]) and the proton-neutron quasiparticle random phase approximation (pn-QRPA) theory (e.g. [16]) were used extensively and with relative success for the microscopic calculation of stellar weak rates. Monte Carlo shell-model is an alternative to the diagonalization method and allows calculation of nuclear properties as thermal averages (e.g. [17]). However it does not allow for detailed nuclear spectroscopy and has some restrictions in its applications for odd-odd and odd-A nuclei.

The pn-QRPA theory is an efficient way to generate GT strength distributions. These strength distributions constitute a primary and nontrivial contribution to the weak-interaction mediated rates among iron-regime nuclide. Because of the high temperatures prevailing during the presupernova and supernova phase of a massive star, there is a reasonable probability of occupation of parent excited states and the total weak interaction rates have a finite contribution form these excited states. The pn-QRPA theory allows a microscopic state-by-state calculation of these rates and this feature of the pn-QRPA model greatly enhances the reliability of the calculated rates in stellar matter.

Nabi and Klapdor-Kleingrothaus [18] first reported the calculation of weak interaction rates for 709 nuclei with A = 18 to 100 in stellar environment using the pn-QRPA theory. These included capture rates, decay rates, neutrino energy loss rates, probabilities of beta-delayed particle emissions and energy rate of these particle emissions. The authors then presented a detailed calculation of stellar weak interaction rates over a wide range of temperature and density scale for sd- [19] and fp/fpg-shell nuclei [16]. These included the weak interaction rates for nuclei with A = 40 to 44 (not yet calculated by shell model). Since then these calculations were further refined with use of more efficient algorithms, computing power, incorporation of latest data from mass compilations and experimental values, and fine-tuning of model parameters [20, 21, 22, 23, 24]. There is a considerable amount of uncertainty involved in all types of calculations of stellar weak interactions. The uncertainty associated with the microscopic calculation of the pn-QRPA model was discussed in detail in Ref. [25]. The reliability of the pn-QRPA calculation was discussed in length by Nabi and Klapdor-Kleingrothaus [16]. There the authors compared the measured data (half lives and B($GT_{\pm}$) strength) of thousands of nuclide with the pn-QRPA calculation and got fairly good comparison. This also encouraged the use of the pn-QRPA model for nuclei where experimental data were not available [26].

Three key isotopes of iron, ^{54,55,56}Fe, were selected for the calculation of neutrino and antineutrino energy loss rates in stellar matter in this part of the project. Aufderheide and collaborators [14] ranked ^{54,55,56}Fe amongst the most influential nuclei with respect to their importance for the electron capture process for the early presupernova collapse. Later Heger et al. [27] studied the presupernova evolution of massive stars (of masses $15M_{\odot}, 25M_{\odot}$, and $40M_{\odot}$) and rated ^{54,55,56}Fe amongst top seven nuclei considered to be most important for decreasing Y_e in $15M_{\odot}$ and $40M_{\odot}$ stars. In $25M_{\odot}$ stars these isotopes of iron were ranked as the top three key nuclei that play the biggest role in decreasing Y_e. These isotopes of iron are mainly responsible for decreasing the electron-to-baryon ratio during the oxygen and silicon burning phases. Besides, ^{55}Fe was also found to be in the top five list of nuclei that increase Y_e via positron capture and electron decay during the silicon burning phases. Earlier the calculation of GT$_{\pm}$ strength distributions and associated stellar electron and positron capture rates for these isotopes of iron were presented using the pn-QRPA model [26]. There I was able to reproduce fairly well the experimental centroids and the total strength distributions in both directions (in the GT$_{+}$ direction a proton is converted to a neutron, as in electron capture or positron decay and in the GT$_{-}$ direction a neutron is converted to a proton, as in positron capture or beta decay) for the even-even iron isotopes, ^{54,56}Fe. No such measured data were available for ^{55}Fe. The calculation of capture rates for these iron isotopes and comparisons with earlier calculations were also presented in Ref. [26]. In this paper I intend to report on the calculation of neutrino and anti-neutrino energy loss rates due to these key isotopes of iron. At lower temperatures and densities characteristic of the hydrostatic phases of stellar evolution, accurate and reliable stellar weak rates are required to determine the nucleosynthesis of nuclear species, the overall neutrino energy loss rates which may affect the temperature of the core (at relevant temperatures and densities the nonthermal neutrinos are transparent to the stellar matter), and the detailed Y_e which becomes very important going into the core collapse. For the later phases of silicon burning to the collapse phase, overall neutronisation rates and neutrino production rates become the most interesting quantities [13] (during this phase the total GT$_{\pm}$ strengths become more important rather than their distributions).

The paper is written in the following format. Section 2 describes the essential formalism for the calculation of neutrino and antineutrino energy loss rates using the pn-QRPA model. I present my calculation in Section 3 where I also compare them with earlier calculations of neutrino energy loss rates. I summarize the main points and conclude finally in Section 4.

2 Basic formalism for pn-QRPA calculation

The QRPA theory considers the residual correlations among the nucleons via one particle one hole (1p-1h) excitations in a large model space and is an efficient way to generate GT strength distributions. Kar et al. [28] pointed out much earlier that the quasiparticle random phase approximation (QRPA) method is quite successful in predicting the weak interaction rates of

ground states all over the periodic table and also stressed the need to extend these methods to non-zero temperature domains relevant to presupernova and supernova conditions. Nabi and Klapdor-Kleingrothaus [18] later used the pn-QRPA model in stellar matter to calculate contributions to weak interaction rates from parent excited states.

The Hamiltonian for this calculation was of the form

$$H^{QRPA} = H^{sp} + V^{pair} + V^{ph}_{GT} + V^{pp}_{GT}. \tag{1}$$

Single particle (sp) energies and wave functions were calculated in the Nilsson model, which takes into account nuclear deformations. Pairing was treated in the BCS approximation. Two types of proton-neutron residual interactions were incorporated in the calculation namely the particle-hole, V^{ph}_{GT}, and the particle-particle, V^{pp}_{GT}, interaction. The two interactions (separable in form) were characterized by two interaction constants: χ (for particle-hole interaction) and κ (for particle-particle interaction). In this work, the values of χ and κ were taken as 0.15 MeV and 0.07 MeV, respectively (the reader is referred to [29, 30] for details of choice of these parameters). Other parameters required for the calculation of weak rates are the pairing gaps, the deformation and the Q-value of the nuclear reactions. The calculated half-lives depend only weakly on the values of the pairing gaps [31] and as such the traditional choice of $\Delta_p = \Delta_n = 12/\sqrt{A}(MeV)$ was applied in the present work. The deformation parameter is as an important parameter for QRPA calculations as pairing [32]. As such rather than using deformations from some theoretical mass model (as used in earlier calculations of pn-QRPA rates) the experimentally adopted value of the deformation parameters for ^{54,56}Fe, extracted by relating the measured energy of the first 2^+ excited state with the quadrupole deformation, was taken from Raman et al. [33]. For the case of ^{55}Fe (where such measurement lacks) the deformation of the nucleus was calculated as

$$\delta = \frac{125(Q_2)}{1.44(Z)(A)^{2/3}}, \tag{2}$$

where Z and A are the atomic and mass numbers, respectively, and Q_2 is the electric quadrupole moment taken from Ref. [34]. Q-values were taken from the recent mass compilation of Audi et al. [35].

The incorporation of measured deformations for ^{54,56}Fe lead to an improvement of the calculated GT$_\pm$ distributions compared to the measured ones. In order to further increase the reliability of the calculated rates experimental data were incorporated in the calculation wherever possible. The calculated excitation energies (along with their log ft values) were replaced with an experimental one when they were within 0.5 MeV of each other. Missing measured states were inserted and inverse and mirror transitions were also taken into account. No theoretical levels were replaced with the experimental ones beyond the excitation energy for which experimental compilations had no definite spin and/or parity. A state-by-state calculation of GT$_\pm$ strength was performed for a total of 246 parent excited states in ^{54}Fe, 297 states for ^{55}Fe and 266 states for ^{56}Fe. For each parent excited state, transitions were calculated for 150 daughter excited states

using the pn-QRPA model. The use of a separable interaction assisted in the incorporation of a luxurious model space of up to 7 major oscillator shells ($7\hbar\omega$) which in turn made possible to consider these many excited states in both parent and daughter nuclei.

The neutrino (antineutrino) energy loss rates can occur through four different weak-interaction mediated channels: electron and positron emissions, and, continuum electron and positron captures. The neutrino energy loss rates were calculated using the formula

$$\lambda_{ij}^{\nu(\bar{\nu})} = \left[\frac{\ln 2}{D}\right] \left[f_{ij}^{\nu}(T,\rho,E_f)\right] \left[B(F)_{ij} + \left(g_A/g_V\right)_{eff}^2 B(GT)_{ij}\right]. \tag{3}$$

The value of D was taken to be 6295s [36]. $B'_{ij}s$ are the sum of reduced transition probabilities of the Fermi B(F) and GT transitions B(GT). The effective ratio of axial and vector coupling constants, $(g_A/g_V)_{eff}$, which takes into account the observed quenching of the GT strength [37] was taken to be [38]:

$$\left(\frac{g_A}{g_V}\right)_{eff}^2 = 0.60 \left(\frac{g_A}{g_V}\right)_{bare}^2, \tag{4}$$

with $(g_A/g_V)_{bare}$ = -1.254 [39]. Interestingly, Vetterli and collaborators [40] and Rönnqvist et al. [41] predicted the same quenching factor of 0.6 for the RPA calculation in the case of ^{54}Fe when comparing their measured strengths to RPA calculation.

The f_{ij}^{ν} are the phase space integrals and are functions of stellar temperature (T), density (ρ) and Fermi energy (E_f) of the electrons. They are explicitly given by

$$f_{ij}^{\nu} = \int_1^{w_m} w\sqrt{w^2-1}(w_m - w)^3 F(\pm Z, w)(1 - G_{\mp})dw, \tag{5}$$

and by

$$f_{ij}^{\nu} = \int_{w_l}^{\infty} w\sqrt{w^2-1}(w_m + w)^3 F(\pm Z, w) G_{\mp} dw. \tag{6}$$

In above equation w is the total energy of the electron including its rest mass, w_l is the total capture threshold energy (rest+kinetic) for positron (or electron) capture. F($\pm$ Z,w) are the Fermi functions and were calculated according to the procedure adopted by Gove and Martin [42]. $G_{\pm}$ is the Fermi-Dirac distribution function for positrons (electrons).

$$G_+ = \left[\exp\left(\frac{E+2+E_f}{kT}\right) + 1\right]^{-1}, \tag{7}$$

$$G_- = \left[\exp\left(\frac{E-E_f}{kT}\right) + 1\right]^{-1}, \tag{8}$$

here E is the kinetic energy of the electrons and k is the Boltzmann constant.

For the decay channel Eq. 5 was used for the calculation of phase space integrals. Upper signs were used for the case of electron emissions and lower signs for the case of positron emissions. Regarding the capture channels, I used Eq. 6 for the calculation of phase space integrals keeping upper signs for continuum electron captures and lower signs for continuum positron captures. Details of the calculation of reduced transition probabilities can be found in Ref. [19].

The total neutrino energy loss rate per unit time per nucleus is given by

$$\lambda^{\nu} = \sum_{ij} P_i \lambda_{ij}^{\nu}, \tag{9}$$

where λ_{ij}^{ν} is the sum of the electron capture and positron decay rates for the transition $i \rightarrow j$ and P_i is the probability of occupation of parent excited states which follows the normal Boltzmann distribution.

On the other hand the total antineutrino energy loss rate per unit time per nucleus is given by

$$\lambda^{\bar{\nu}} = \sum_{ij} P_i \lambda_{ij}^{\bar{\nu}}, \tag{10}$$

where $\lambda_{ij}^{\bar{\nu}}$ is the sum of the positron capture and electron decay rates for the transition $i \rightarrow j$.

The summation over all initial and final states was carried out until satisfactory convergence in the rate calculation was achieved. The pn-QRPA theory allows a microscopic state-by-state calculation of both sums present in Eqts. 9 and 10. This feature of the pn-QRPA model greatly increases the reliability of the calculated rates in stellar matter where there exists a finite probability of occupation of excited states.

3 Results and comparison

The calculation of $GT_{\pm}$ strength distributions for ^{54,55,56}Fe was presented and discussed in detail in Ref. [26]. There I also compared the calculated strength functions against the measured distributions for the case of even-even isotopes of iron. Here I present the cumulative $B(GT_{\pm})$ strength distributions for ^{54,55,56}Fe using the pn-QRPA model. Figs. 1-3 display the cumulative $B(GT_{+})$ strength distributions for the three isotopes of iron. For the case of the even-even isotopes (where measured distributions exist) I display the experimental results in inset. The measured GT_{+} distribution for ^{54}Fe was taken from Ref. [41]. One should note the peak in the strength distribution of ^{54}Fe around 7 MeV (Fig. 1). For both the cases of ^{54,56}Fe the pn-QRPA distributions spread over higher excitation energies (around 10 MeV in daughter) akin to measured strengths. For the case of ^{56}Fe, the experimental data were taken from Ref. [43]. Similarly the cumulative $B(GT_{-})$ strength distributions for the iron isotopes are displayed in Figs. 4-6. One curious finding of Ref. [26] was that $GT_{\pm}$ strength distributions from low-lying excited states in parent nucleus are much different from the corresponding ground-state distributions. In stellar environments there is a finite contribution to the total weak rates from these parent excited states. Earlier calculations of weak interaction rates, including those of FFN [13] and large-scale shell model [15] calculation, incorporated the distributions from excited states by using the so-called Brink's hypothesis in the electron capture direction (it is to be noted that the LSSM calculation is also capable of performing a microscopic calculation of GT strength distribution albeit for a few low-lying states not exceeding 1 MeV in parent nucleus) and back-resonances in

the β-decay direction. Brink's hypothesis states that GT strength distribution on excited states is *identical* to that from ground state, shifted *only* by the excitation energy of the state. GT back resonances are the states reached by the strong GT transitions in the inverse process (electron capture) built on ground and excited states. The pn-QRPA model has the advantage that these excited state distributions can be calculated in a microscopic fashion. Table 1 shows the values of the calculated centroids and total strengths $\Sigma S_{\beta^{\pm}}$ (in both directions) for ground and first two excited states of ^{54,55,56}Fe. The energies (in daughter) are given in units of MeV and the GT strengths are given in units such that B(GT) = 3 for neutron decay. The centroids of the $GT_{\pm}$ strength distributions are shifted to higher excitation energies in daughter nuclei for the excited states as compared to the ground state centroids (not so appreciably for the case of ^{55}Fe). The total strengths $\Sigma S_{\beta^{\pm}}$ also change appreciably for the excited states. These changes have an effect on the calculated rates specially at low temperatures and densities (where specific low-lying transitions may dominate the rate calculation). The rate contributions from parent excited states were calculated and explicitly displayed in Table III of Ref. [26].

Moving on to the calculation of neutrino energy loss rates, Figs. 7-9 depict the energy loss rates for ^{54}Fe, ^{55}Fe and ^{56}Fe, respectively. Each figure consists of four panels depicting the calculated neutrino energy loss rates at selected temperature and density domain. It is pertinent to mention again that the neutrino energy loss rates contain contributions due to electron capture *and* positron decay on iron isotopes. The upper left panel, in all figures, shows the energy loss rates in low-density region ($\rho[gcm^{-3}] = 10^{0.5}, 10^{1.5}$ and $10^{2.5}$), the upper right in medium-low density region ($\rho[gcm^{-3}] = 10^{3.5}, 10^{4.5}$ and $10^{5.5}$), the lower left in medium-high density region ($\rho[gcm^{-3}] = 10^{6.5}, 10^{7.5}$ and $10^{8.5}$) and finally the lower right panel depicts the calculated rates in high density region ($\rho[gcm^{-3}] = 10^{9.5}, 10^{10.5}$ and 10^{11}). The neutrino energy loss rates are given in logarithmic scales (to base 10) in units of $MeV.s^{-1}$. In the figures T_9 gives the stellar temperature in units of 10^9 K. One should note the order of magnitude differences in neutrino energy loss rates as the stellar temperature increases specially in the case of ^{56}Fe (Fig. 9). For densities $\rho[gcm^{-3}] \leq 10^{8.5}$, the pn-QRPA calculates the lowest energy loss rates due to ^{56}Fe (Fig. 9) at low temperatures ($T_9 \leq 5$) and highest due to ^{55}Fe (Fig. 8). It can be seen from these figures that in the low density region the energy loss rates, as a function of stellar temperatures, are more or less superimposed on one another. This means that there is no appreciable change in the neutrino energy loss rates when increasing the density by an order of magnitude. There is a sharp exponential increase in the neutrino energy loss rates for the low, medium-low and medium-high density regions as the stellar temperature increases up to T_9 =5. Beyond this temperature the slope of the rates reduces drastically with increasing density. For a given temperature the neutrino energy loss rates increase monotonically with increasing densities.

The calculated antineutrino energy loss rates contain contributions due to positron capture *and* β-decay on iron isotopes (see Eq. 10). Figs. 10-12 show a similar calculation for the antineutrino energy loss rates for the selected isotopes of iron. Here one notes that the corresponding

rates are much smaller. Again one notes that the rates increase very sharply until T_9 approaches 5. The rates are almost superimposed on one another as a function of stellar densities. However as the stellar matter moves from the medium high density region to high density region these rates start to 'peel off' from one another. The neutrino and antineutrino energy loss rates are calculated on an extensive temperature-density grid point suitable for collapse simulations and the electronic versions of these files may be requested from the author.

An interesting question would be to know how the pn-QRPA calculation compares with large-scale shell model (LSSM) calculation [15] and the pioneer calculation done by FFN [13] (specially for temperature and density domains of astrophysical interest) for these key iron isotopes. The comparisons are presented in a tabular form. Tables (2 – 4) show the comparison of calculated neutrino energy loss rates with those of FFN and LSSM for ^{54}Fe, ^{55}Fe and ^{56}Fe, respectively. Here the ratios of the calculated neutrino energy loss rates to those of LSSM, R_ν(LSSM), and the corresponding ratios to those of FFN, R_ν(FFN), are presented at selected temperature and density points. According to the study of presupernova evolution by Heger and collaborators [27], electron capture rates on ^{54}Fe are important from the oxygen shell burning phase up to the end of convective core silicon burning phase of massive stars. For temperatures ($T_9 \sim 1$) and densities ($\rho \sim 10^7 gcm^{-3}$) corresponding roughly to the oxygen shell burning phase of massive stars, the calculated neutrino energy loss rates due to ^{54}Fe are slightly enhanced by around a factor of four compared to LSSM results (Table 2). During this important phase of stellar evolution the pn-QRPA neutrino energy loss rates are generally in good agreement with the LSSM rates. As the temperature and density increase the comparison with LSSM results gets better and better. The calculated energy loss rates due to ^{54}Fe are up to an order of magnitude smaller in the same region as compared to FFN rates. The comparison improves at higher temperatures. It is to be noted that FFN neglected the quenching of the total GT strength in their rate calculation.

The electron capture rates on ^{55}Fe are most effective during the oxygen shell burning till around the ignition of the first stage of convective silicon shell burning of massive stars [27]. Correspondingly one should expect the most effective cooling contribution due to ^{55}Fe during the above mentioned phases of stellar evolution. For the corresponding temperatures ($T_9 \sim 3$) and densities ($\rho \sim 10^7 gcm^{-3}$), the pn-QRPA rates are bigger than LSSM rates by more than an order of magnitude (Table 3). It is to be noted that the reported rates are enhanced by more than an order of magnitude at low temperatures as compared to LSSM numbers and favor cores with lower entropy. At higher temperatures and densities the comparison gets better with LSSM results whereas FFN rates are bigger than the LSSM and pn-QRPA rates by roughly an order of magnitude for reasons mentioned before.

The comparison of calculated electron capture rates was remarkably good against the LSSM rates for the case of ^{56}Fe for all temperature and density points [26]. A similarly good comparison is also witnessed for the case of neutrino energy loss rates due to ^{56}Fe against the LSSM numbers (Table 4). FFN rates are again enhanced by a factor of two to four as compared to pn-QRPA

and LSSM rates.

4 Summary and conclusions

In order to understand the supernova explosion mechanism international collaborations of astronomers and physicists are being sought. Weak interaction mediated rates are key nuclear physics input to simulation codes and a reliable and microscopic calculation of these rates (both from ground-state *and* excited states) is desirable. The pn-QRPA model was used to calculate the (anti)neutrino energy loss rates due to iron isotopes in stellar matter. The calculation was performed in a luxurious model space of $7\hbar\omega$. The microscopic state-by-state calculation of $GT_{\pm}$ strength distributions from ground and excited states highlighted the fact that the Brink's hypothesis and back resonances may not be a good approximation to use in stellar calculation of weak rates.

The associated energy loss rates due to weak interactions on iron isotopes in stellar matter were also calculated using the pn-QRPA theory. Deformations of nuclei were taken into account and the calculation took into consideration the experimental deformations for even-even isotopes of iron (^{54,56}Fe). Maximum possible experimental data were incorporated to enhance the reliability of calculated results. The calculated neutrino energy loss rates due to ^{54,56}Fe are, generally, in good agreement with the LSSM rates during the oxygen and silicon shell burning phases of massive stars. The comparison with LSSM gets better for pre-supernova and supernova phases of stellar evolution. During silicon shell burning for stars ($\sim 10 - 25 M_{\odot}$) and oxygen shell burning for much heavier stars ($\sim 40 M_{\odot}$) the calculated energy loss rates due to ^{55}Fe are up to more than one order of magnitude bigger than LSSM rates.

According to the study of presupernova evolution by authors in Ref. [27] the most important period for determining core structure and lepton fraction in the core occurs during silicon shell burning. During this decisive phase of stellar evolution the pn-QRPA calculated energy loss rates due to ^{55}Fe are much enhanced as compared to the results of large-scale shell model calculation and favor cooler cores with lower entropies. This information may be of use for core-collapse simulators and may contribute in the fine tuning of the temperature, entropy and the lepton-to-baryon ratio which become very important going into stellar collapse. The rates are calculated on an extensive temperature-density grid point suitable for collapse simulations and the electronic versions of these files may be requested from the author.

Acknowledgments

This work was done within the framework of the Associateship Scheme of the Abdus Salam International Centre for Theoretical Physics, Trieste, Italy.

References

[1] S. A. Colgate and R. White, Astrophys. J. 143 (1966) 626.

[2] W. D. Arnett, Canadian J. Phys. 45 (1967) 1621.

[3] H. A. Bethe and J. R. Wilson, Astrophys. J. 295 (1985) 14.

[4] R. Buras, M. Rampp, H. T. Janka and K. Kifonidis, Phys. Rev. Lett. 90 (2003) 241101.

[5] C. L. Fryer, Astrophys. J. 522 (1999) 413.

[6] K. Kotake, H. Sawai, S. Yamada and K. Sato, Astrophys. J. 608 (2004) 391.

[7] R. Walder, A. Burrows, C. D. Ott, E. Livne, I. Lichtenstadt and M. Jarrah, Astrophys. J. 623 (2005) 317.

[8] W. C. Haxton, Phys. Rev. Lett. 60 (1988) 1999.

[9] S. W. Bruenn and W. C. Haxton, Astrophys. J. 376 (1991) 678.

[10] K. Langanke, G. Martínez-Pinedo, B. Müller, H.-Th Janka, A. Marek, W. R. Hix, A. Juodagalvis, and J. M. Sampaio, Phys. Rev. Lett. 100 (2008) 011101.

[11] W. Haxton, private communication.

[12] S. Esposito, G. Mangano, G. Miele, I. Picardi and O. Pisanti, Nucl. Phys. B 658 (2003) 217.

[13] G. M. Fuller, W. A. Fowler, and M. J. Newman, Astrophys. J. Suppl. Ser 42 (1980) 447; 48 (1982) 279; Astrophys. J. 252 (1982) 715; 293 (1985) 1.

[14] M. B. Aufderheide, I. Fushiki, S. E. Woosley, E. Stanford, and D. H. Hartmann, Astrophys. J. Suppl. 91 (1994) 389.

[15] K. Langanke and G. Martínez-Pinedo, Nucl. Phys. A 673 (2000) 481.

[16] J.-U. Nabi and H. V. Klapdor-Kleingrothaus, At. Data Nucl. Data Tables 88 (2004) 237.

[17] C. W. Johnson, S. E. Koonin, G. H. Lang, and W. E. Ormand, Phys. Rev. Lett. 69 (1992) 3157.

[18] J.-U. Nabi and H. V. Klapdor- Kleingrothaus, Eur. Phys. J. A 5 (1999) 337.

[19] J.-U. Nabi and H. V. Klapdor-Kleingrothaus, At. Data Nucl. Data Tables 71 (1999) 149.

[20] J.-U. Nabi and M.-U. Rahman, Phys. Rev. C 75 (2007) 035803.

[21] J.-U. Nabi, M. Sajjad, and M.-U. Rahman, Acta. Phys. Polon. B 38 (2007) 3203.

[22] J.-U. Nabi and M. Sajjad, Phys. Rev. C 76 (2007) 055803.

[23] J.-U. Nabi, M.-U. Rahman, and M. Sajjad, Acta. Phys. Polon. B 39 (2008) 651.

[24] J.-U. Nabi and M. Sajjad, to appear in Can. J. Phys. (2008).

[25] J.-U. Nabi and M. Sajjad, Phys. Rev. C 77 (2008) 055802.

[26] J.-U. Nabi, to be submitted (2008).

[27] A. Heger, S. E. Woosley, G. Martínez-Pinedo, and K. Langanke, Astrophys. J. 560 (2001) 307.

[28] K. Kar, R. Ray and S. Sarkar, Astrophys. J. 433 (1994) 662.

[29] A. Staudt, E. Bender, K. Muto, and H. V. Klapdor-Kleingrothaus, At. Data Nucl. Data Tables 44 (1990) 79.

[30] M. Hirsch, A. Staudt, K. Muto, and H. V. Klapdor-Kleingrothaus, At. Data Nucl. Data Tables 53 (1993) 165.

[31] M. Hirsch, A. Staudt, K. Muto, and H. V. Klapdor-Kliengrothaus, Nucl. Phys. A535 (1991) 62.

[32] I. Stetcu and C. W. Johnson, Phys. Rev. C 69 (2004) 024311.

[33] S. Raman, C. H. Malarkey, W. T. Milner, C. W. Nestor, Jr., and P. H. Stelson, At. Data Nucl. Data Tables 36 (1987) 1.

[34] P. Möller and J. R. Nix, At. Data Nucl. Data Tables 26 (1981) 165.

[35] G. Audi, A. H. Wapstra, and C. Thibault, Nucl. Phys. A729 (2003) 337.

[36] G. P. Yost *et al.* (Particle Data Group), Phys. Lett. B204 (1988) 1.

[37] F. Osterfeld, Rev. Mod. Phys. 64 (1992) 491.

[38] C. Gaarde, Nucl. Phys. A 396 (1983) 127c.

[39] V. Rodin, A. Faessler, F. Simkovic, and P. Vogel, Czech. J. Phys. 56 (2006) 495.

[40] M. C. Vetterli, O. Häusser, R. Abegg, W. P. Alford, A. Celler, D. Frekers, R. Helmer, R. Henderson, K. H. Hicks, K. P. Jackson, R. G. Jeppesen, C. A. Miller, K. Raywood, and S. Yen, Phys. Rev. C 40 (1989) 559.

[41] T. Rönnqvist, H. Condé, N. Olsson, E. Ramström, R. Zorro, J. Blomgren, A. Håkansson, A. Ringbom, G. Tibell, O. Jonsson, L. Nilsson, P.-U. Renberg, S. Y. van der Werf, W. Unkelbach, and F. P. Brady, Nucl. Phys. A563 (1993) 225.

[42] N. B. Gove and M. J. Martin, At. Data Nucl. Data Tables 10 (1971) 205.

[43] S. El-Kateb, K. P. Jackson, W. P. Alford, R. Abegg, R. E. Azuma, B. A. Brown, A. Celler, D. Frekers, O. Häusser, R. Helmer, R. S. Henderson, K. H. Hicks, R. Jeppesen, J. D. King, K. Raywood, G. G. Shute, B. M. Spicer, A. Trudel, M. Vetterli, and S. Yen, Phys. Rev. C 49 (1994) 3128.

Table 1: Comparison of pn-QRPA calculated energy centroids and total GT strengths (in both directions) for the ground and first two excited states of $^{54,55,56}Fe$. For units see text.

States	E(GT_+)	E(GT_-)	$\Sigma S_{\beta+}$	$\Sigma S_{\beta-}$
^{54}Fe (ground)	4.06	5.08	4.26	7.56
^{54}Fe (1^{st})	7.10	7.81	5.12	6.97
^{54}Fe (2^{nd})	7.48	8.23	3.84	9.23
^{55}Fe (ground)	6.92	8.28	4.81	6.87
^{55}Fe (1^{st})	7.38	8.56	4.43	8.87
^{55}Fe (2^{nd})	7.40	8.83	5.03	6.87
^{56}Fe (ground)	3.13	5.61	3.71	10.74
^{56}Fe (1^{st})	6.17	8.89	5.15	8.04
^{56}Fe (2^{nd})	6.74	8.76	4.15	10.21

Table 2: Ratios of calculations of neutrino energy loss rates due to ^{54}Fe at different selected densities and temperatures. R_ν denotes the ratio of the calculated neutrino energy loss rates to those calculated by large scale shell model (LSSM) and those calculated by Fuller and collaborators (FFN).

T_9	R_ν(LSSM)	R_ν(FFN)	R_ν(LSSM)	R_ν(FFN)	R_ν(LSSM)	R_ν(FFN)	R_ν(LSSM)	R_ν(FFN)
	$10gcm^{-3}$	$10gcm^{-3}$	10^3gcm^{-3}	10^3gcm^{-3}	10^7gcm^{-3}	10^7gcm^{-3}	$10^{11}gcm^{-3}$	$10^{11}gcm^{-3}$
1	4.68E+00	9.66E-02	4.69E+00	9.66E-02	3.96E+00	1.13E-01	8.32E-01	2.96E-01
3	2.37E+00	1.48E-01	2.37E+00	1.48E-01	2.47E+00	1.71E-01	8.30E-01	2.95E-01
10	8.15E-01	3.90E-01	8.12E-01	3.91E-01	8.34E-01	3.94E-01	8.11E-01	2.90E-01
30	1.05E+00	3.60E-01	1.05E+00	3.61E-01	1.05E+00	3.61E-01	1.01E+00	3.51E-01

Table 3: Same as Table 2, but for neutrino energy loss rates due to ^{55}Fe.

T_9	R_ν(LSSM)	R_ν(FFN)	R_ν(LSSM)	R_ν(FFN)	R_ν(LSSM)	R_ν(FFN)	R_ν(LSSM)	R_ν(FFN)
	$10gcm^{-3}$	$10gcm^{-3}$	10^3gcm^{-3}	10^3gcm^{-3}	10^7gcm^{-3}	10^7gcm^{-3}	$10^{11}gcm^{-3}$	$10^{11}gcm^{-3}$
1	3.27E+01	3.18E+01	3.27E+01	3.19E+01	3.30E+01	3.27E+01	8.85E-01	1.77E-01
3	9.86E+00	2.43E+00	9.89E+00	2.43E+00	1.30E+01	2.82E+00	8.57E-01	1.74E-01
10	1.20E+00	1.67E-01	1.20E+00	1.67E-01	1.22E+00	1.67E-01	8.67E-01	1.84E-01
30	1.68E+00	3.33E-01	1.69E+00	3.33E-01	1.69E+00	3.34E-01	1.43E+00	3.27E-01

Table 4: Same as Table 2, but for neutrino energy loss rates due to ^{56}Fe.

T_9	R_ν(LSSM)	R_ν(FFN)	R_ν(LSSM)	R_ν(FFN)	R_ν(LSSM)	R_ν(FFN)	R_ν(LSSM)	R_ν(FFN)
	$10gcm^{-3}$	$10gcm^{-3}$	10^3gcm^{-3}	10^3gcm^{-3}	10^7gcm^{-3}	10^7gcm^{-3}	$10^{11}gcm^{-3}$	$10^{11}gcm^{-3}$
1	8.49E-01	2.61E-01	8.49E-01	2.61E-01	9.75E-01	3.15E-01	1.08E+00	3.57E-01
3	1.04E+00	2.36E-01	1.04E+00	2.37E-01	1.08E+00	2.44E-01	1.05E+00	3.51E-01
10	8.75E-01	4.57E-01	8.77E-01	4.58E-01	8.83E-01	4.59E-01	9.95E-01	3.30E-01
30	1.13E+00	4.56E-01	1.13E+00	4.57E-01	1.13E+00	4.58E-01	1.26E+00	4.17E-01

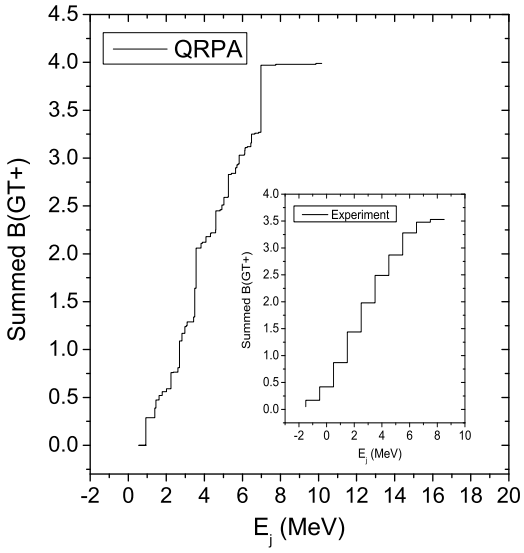

Figure 1: Cumulative sum of the $B(GT_+)$ values for ^{54}Fe. The energy scale refers to excitation energies in daughter ^{54}Mn. Inset displays the corresponding measured cumulative $B(GT_+)$ values [41].

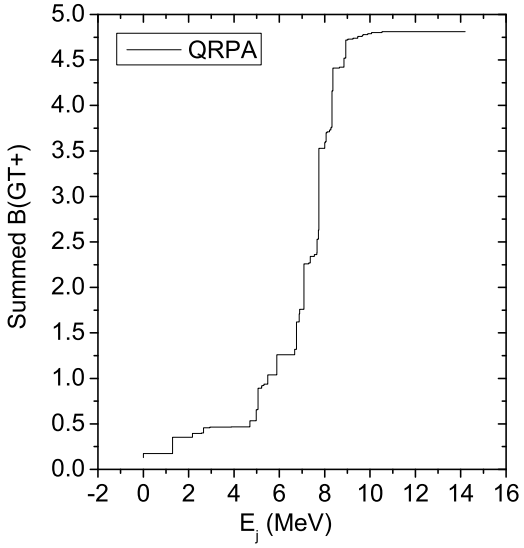

Figure 2: Cumulative sum of the $B(GT_+)$ values for ^{55}Fe. The energy scale refers to excitation energies in daughter ^{55}Mn.

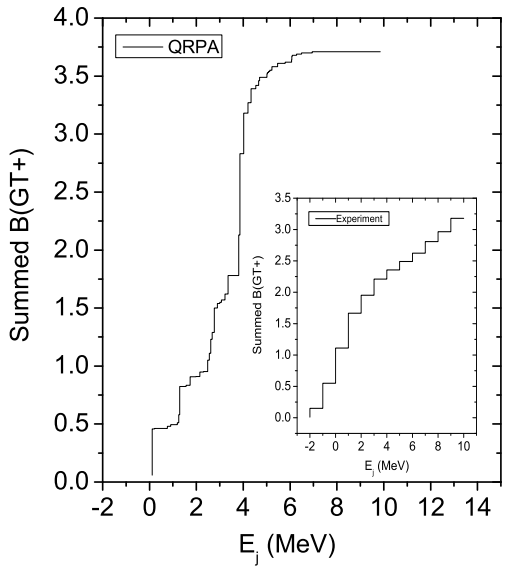

Figure 3: Cumulative sum of the $B(GT_+)$ values for ^{56}Fe. The energy scale refers to excitation energies in daughter ^{56}Mn. Inset displays the corresponding measured cumulative $B(GT_+)$ values [43].

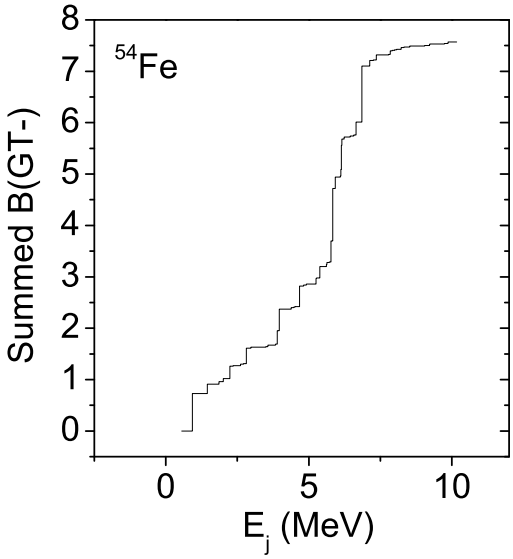

Figure 4: Cumulative sum of the $B(GT_-)$ values for ^{54}Fe. The energy scale refers to excitation energies in daughter ^{54}Co.

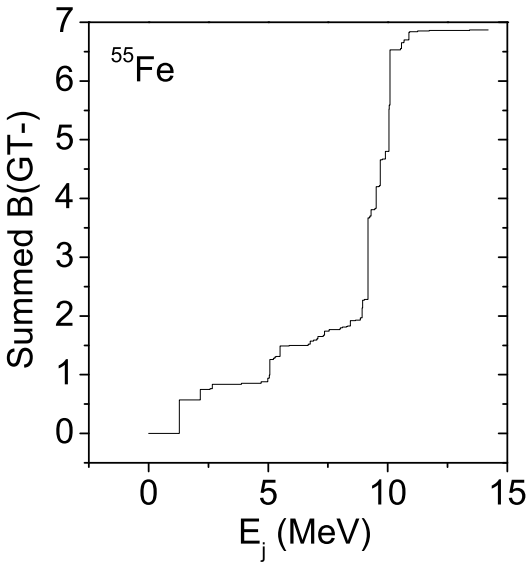

Figure 5: Cumulative sum of the B(GT$_-$) values for ^{55}Fe. The energy scale refers to excitation energies in daughter ^{55}Co.

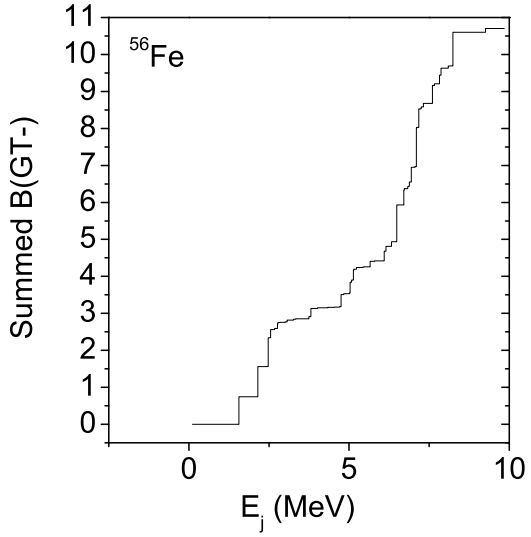

Figure 6: Cumulative sum of the B(GT$_-$) values for ^{56}Fe. The energy scale refers to excitation energies in daughter ^{56}Co.

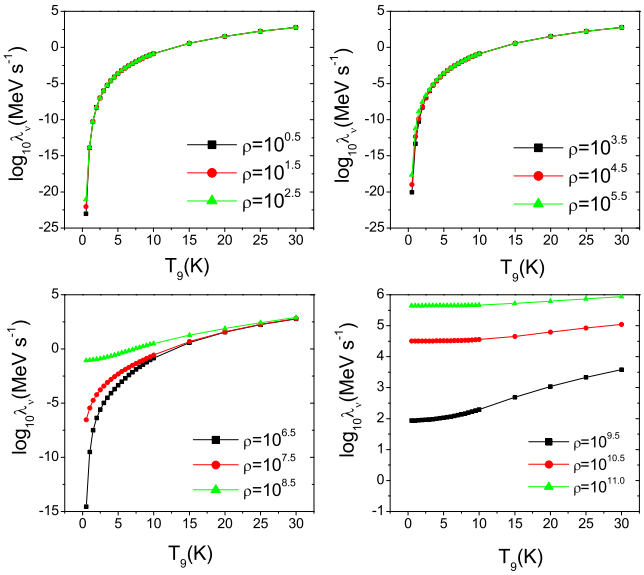

Figure 7: (Color online) Neutrino energy loss rates on ^{54}Fe, as a function of stellar temperatures, for different selected densities. Densities are in units of gcm^{-3}. Temperatures are given in 10^9 K and $\log_{10}\lambda_\nu$ represents the log (to base 10) of neutrino energy loss rates in units of $MeV.sec^{-1}$.

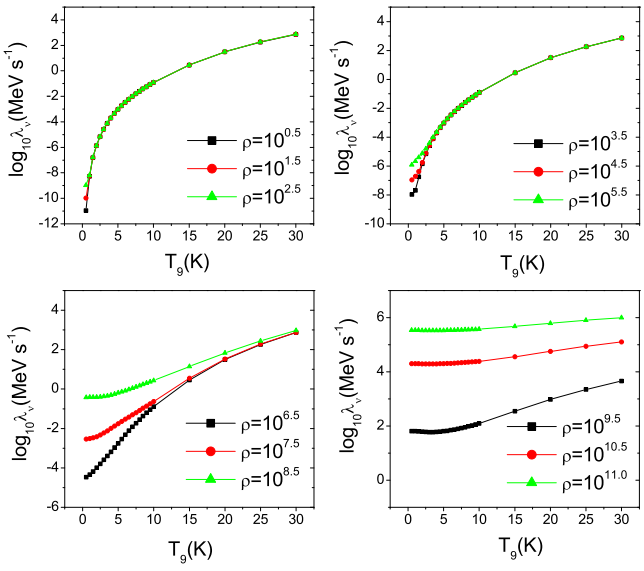

Figure 8: (Color online) Neutrino energy loss rates on ^{55}Fe, as a function of stellar temperatures, for different selected densities. Densities are in units of gcm^{-3}. Temperatures are given in 10^9 K and $\log_{10}\lambda_\nu$ represents the log (to base 10) of neutrino energy loss rates in units of $MeV.sec^{-1}$.

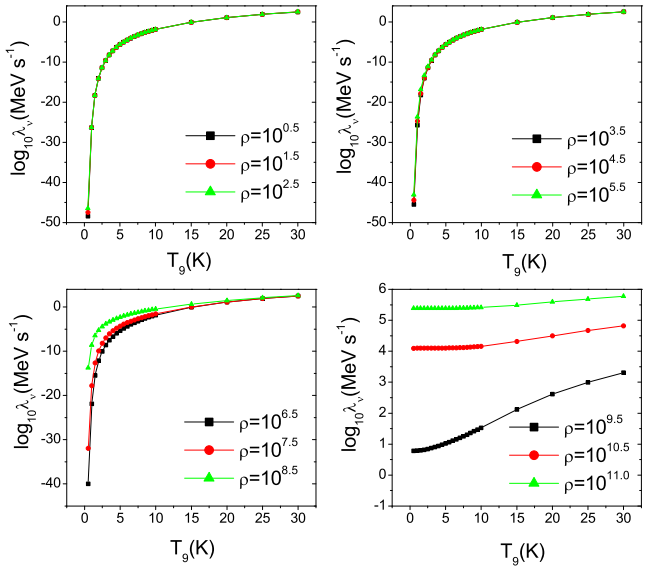

Figure 9: (Color online) Neutrino energy loss rates on ^{56}Fe, as a function of stellar temperatures, for different selected densities. Densities are in units of gcm^{-3}. Temperatures are given in 10^9 K and $\log_{10}\lambda_\nu$ represents the log (to base 10) of neutrino energy loss rates in units of $MeV.sec^{-1}$.

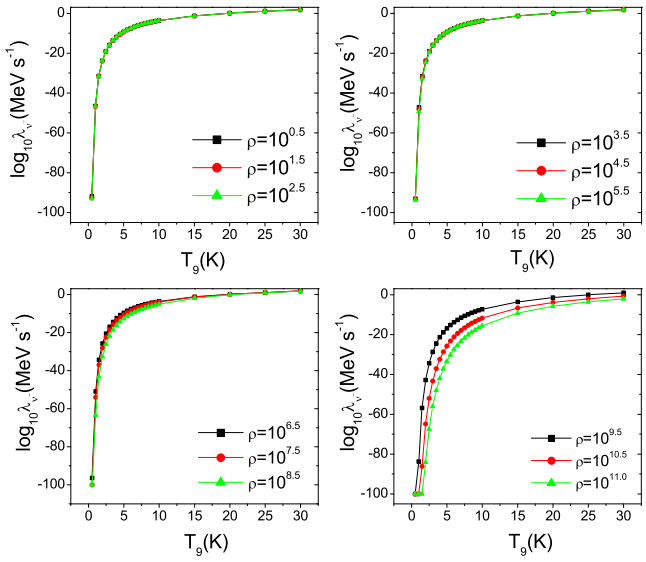

Figure 10: (Color online) Antineutrino energy loss rates on ^{54}Fe, as a function of stellar temperatures, for different selected densities. Densities are in units of gcm^{-3}. Temperatures are given in 10^9 K and $\log_{10}\lambda_{\bar{\nu}}$ represents the log (to base 10) of antineutrino energy loss rates in units of $MeV.sec^{-1}$.

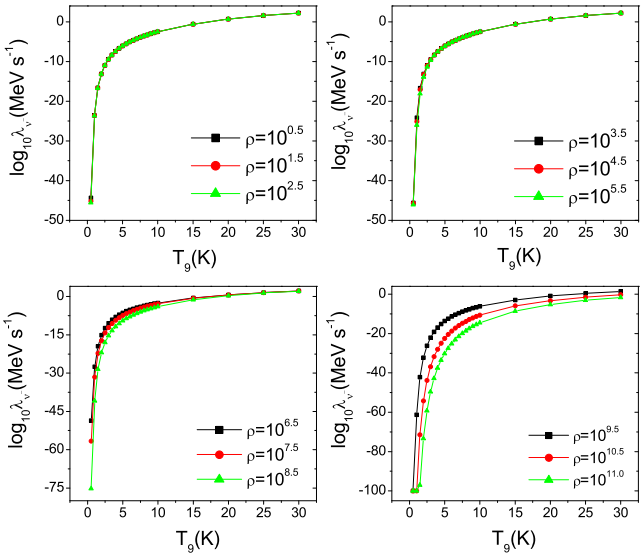

Figure 11: (Color online) Antineutrino energy loss rates on ^{55}Fe, as a function of stellar temperatures, for different selected densities. Densities are in units of gcm^{-3}. Temperatures are given in 10^9 K and $\log_{10}\lambda_{\bar{\nu}}$ represents the log (to base 10) of antineutrino energy loss rates in units of $MeV.sec^{-1}$.

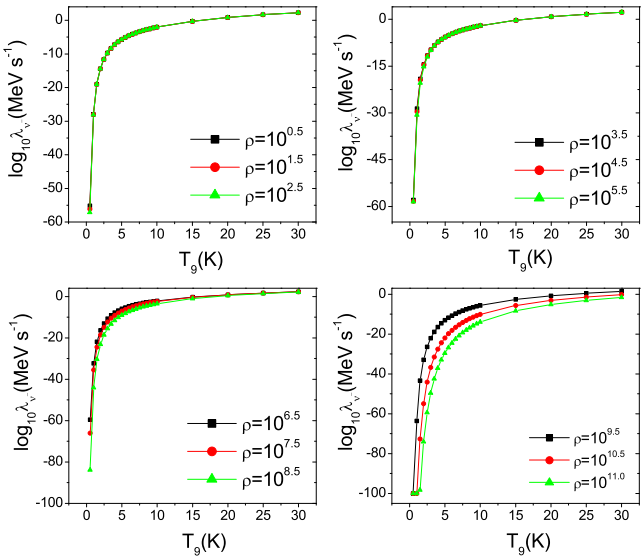

Figure 12: (Color online) Antineutrino energy loss rates on ^{56}Fe, as a function of stellar temperatures, for different selected densities. Densities are in units of gcm^{-3}. Temperatures are given in 10^9 K and $\log_{10}\lambda_{\bar{\nu}}$ represents the log (to base 10) of antineutrino energy loss rates in units of $MeV.sec^{-1}$.